THE JOURNAL OF BIOLOGICAL CHEMISTRY
Vol. 273, No. 4, Issue of January 23, pp. 2199–2206, 1998

Printed in U.S.A.

Triose-phosphate Isomerase (TIM) of the Psychrophilic Bacterium *Vibrio marinus*

KINETIC AND STRUCTURAL PROPERTIES*

(Received for publication, October 14, 1997)

Marco Alvarez‡, Johan Ph. Zeelen§, Véronique Mainfroid‡, Françoise Rentier-Delrue‡, Joseph A. Martial‡, Lode Wyns¶, Rik K. Wierenga§‖, and Dominique Maes¶**

From the ‡Laboratoire de Biologie Moléculaire et de Génie Génétique, Université de Liège, B6, Sart Tilman, B4000 Liège, Belgium, §European Molecular Biology Laboratory, Meyerhofstrasse 1, Postfach 102209, D69012 Heidelberg, Germany, and ¶Ultrastructure Unit, Vlaams Interuniversitair Instituut voor Biotechnologie, Vrije Universiteit Brussel, B1640 Sint-Genesius-Rode, Belgium

The purification and characterization of triose-phosphate isomerase from the psychrophilic bacterium *Vibrio marinus* (vTIM) is described. Crystal structures of the vTIM-sulfate complex and the vTIM-2-phosphoglycolate complex (at a 2.7-Å resolution) are also presented. The optimal growth temperature of *Vibrio marinus* is 15 °C. Stability studies show that vTIM is an unstable protein with a half-life of only 10 min at 25 °C. The vTIM sequence is most closely related to the sequence of *Escherichia coli* TIM (eTIM) (66% identity), and several unique structural features described for eTIM are also seen in vTIM, but eTIM is considerably more stable. The T_d values of vTIM and eTIM, determined by calorimetric studies, are 41 and 54 °C, respectively. Amino acid sequence comparison reveals that vTIM has an alanine in loop 8 (at position 238), whereas all other TIM sequences known to date have a serine. The vTIM mutant A238S was produced and characterized. Compared with wild type, the catalytic efficiency of the A238S mutant is somewhat reduced, and its stability is considerably increased.

Triose-phosphate isomerase (TIM[1]; EC 5.3.1.1) is a dimeric glycolytic enzyme formed by two identical subunits consisting of about 250 residues each. It catalyzes the interconversion of dihydroxyacetone phosphate and D-glyceraldehyde-3-phosphate (see Fig. 1). TIM has been the subject of extensive biophysical, enzymological, and computational studies. Its catalytic properties and mechanism have been studied in detail (1, 2). It has been established that TIM is a very efficient catalyst, since the reaction rates are diffusion-controlled. Neither cofactors nor metal ions are required in this reaction, and there is no evidence of allostery or cooperativity among the subunits.

Structurally TIMs do form a well characterized family. To date, x-ray structures of TIM from seven different sources have been solved (wild type or/and in complex with substrate analogues): chicken (3), yeast (4), *Trypanosoma brucei* (5), *Escherichia coli* (6), human (7), *Bacillus stearothermophilus* (8), and *Plasmodium falciparum* (9). In addition, the structures have been determined of *Leishmania mexicana* TIM[2] and of *Thermotoga maritima* TIM.[3] Also, 45 amino acid TIM sequences from a wide variety of organisms have been determined and are available in the data bases.

Each TIM monomer has a globular shape with two protruding loops. The globular part is formed by an 8-fold repeat of a β-strand, loop, α-helix, loop motif. The $\beta\alpha$ units fold up in a regular way, such that the β-strands (numbered β1 to β8) form an eight-stranded β-barrel surrounded by the eight α-helices (numbered α1 to α8) on the outside. This folding motif is also referred to as the TIM barrel motif. In TIM, the two protruding loops are after β-strand three and after β-strand six.

The TIM barrel structural motif is found for a large number of other enzymes with widely different functions (10) that have little or no sequence homology. As such this stable framework with tolerant sequence variations has already been used as an interesting scaffold to design loops (11, 12) and even artificial proteins (13, 14). The active sites of all these TIM barrel enzymes are located at the C-terminal end of the β-barrel, with catalytic residues contributed by the β-strands and the loops connecting the β-strands to subsequent α-helices numbered loop 1 to loop 8 in correspondence with the numbering of the preceding β-strands. The loops preceding the β-strands are located on the other side of the barrel and are believed to be important for the stability of the TIM barrel (15).

In the TIM dimer, the dimer interface is formed mainly by loops 1, 2, 3, and 4. The protruding loop 3 of one subunit docks into a deep pocket between loop 1 and loop 4 of the other subunit (16). The catalytic residues, a lysine, a histidine, and a glutamate are located in loop 1, loop 4, and loop 6, respectively. Binding of substrate or substrate analogues is accompanied by

* This work was supported by Services Fédéraux des Affaires Scientifiques, Techniques, et Culturelles Grant PAI P3-044, European Union Grants BIOT CT90-0182 and BIO4-CT96-0670, and Belgian National Science Foundation Grant FRFC 2.4545.96. The costs of publication of this article were defrayed in part by the payment of page charges. This article must therefore be hereby marked "*advertisement*" in accordance with 18 U.S.C. Section 1734 solely to indicate this fact.

The nucleotide sequence(s) reported in this paper has been submitted to the GenBank™/EBI Data Bank with accession number(s) U48935.

The atomic coordinates and structure factors (1AW1 and 1AW2) have been deposited in the Protein Data Bank, Brookhaven National Laboratory, Upton, NY.

‖ To whom correspondence may be addressed: European Molecular Biology Laboratory, Meyerhofstrasse 1, Postfach 102209, D69012 Heidelberg, Germany. Tel.: 49 6221 3870256; Fax: 49 6221 387306; E-mail: Rik.wierenga@embl-heidelberg.de.

** A research associate of the Belgian National Science Foundation (FWO) and to whom correspondence may be addressed: ULTR, IMOL, Vrije Universiteit Brussel, Paardenstraat 65, B-1640 Sint-Genesius-Rode, Belgium. Tel.: 32 2 359 0263; Fax: 32 2 359 0289; E-mail: dommaes@vub.ac.be.

[1] The abbreviations used are: TIM, triose-phosphate isomerase; vTIM, eTIM, tTIM, TIM of *V. marinus*, *E. coli*, *T. brucei*, respectively; 2PG, 2-phosphoglycolate; bp, base pair(s).

[2] J. Williams, P. Michels, and R. K. Wierenga, manuscript in preparation.

[3] D. Maes, J. Ph. Zeelen, R. Jaenicke, and R. K. Wierenga, manuscript in preparation. This manuscript will compare all 10 TIM structures and focus on potentially thermostabilizing features.

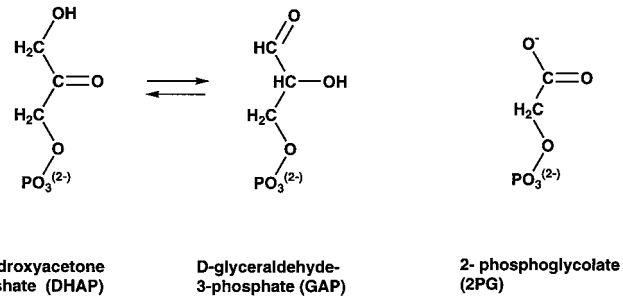

FIG. 1. **The reaction catalyzed by triose-phosphate isomerase, and the covalent structure of the substrate analogue 2PG is shown.**

changes in conformation of loops 5, 6, and 7. The most remarkable change occurs in loop 6, "the flexible loop," the tip of which undergoes a C_α movement of some 7 Å in response to ligand binding (17, 18). As such, the active site is closed off from solvent to prevent an unwanted phosphate elimination reaction that may otherwise occur (1). This state is called "the closed state" in contrast to the unliganded "open state." In the liganded form the oxygen atoms of the phosphate interact with main chain atoms of loops 6, 7, and 8. Loop 8 is called the phosphate binding loop, because it comprises a 3/10 helix (the phosphate binding helix) whose N terminus points directly to the phosphate moiety, allowing for hydrogen bonds between main chain NH groups and phosphate oxygen atoms. These interactions keep the phosphate moiety rigidly in place, whereas in the triose part of the ligand molecule, the catalytic conversion takes place.

The glutamate at the beginning of loop 6 is implicated in the transfer of a proton between the two substrate C atoms. The side chain of this glutamate can occupy two different positions, depending on the contents of the active site. In ligand-free TIM, it is found in a "swung out" conformation, whereas in liganded TIM, it occupies a "swung in" conformation, ideal for carrying out catalysis (19).

In this paper, we focus on the TIM enzyme from the psychrophilic bacterium *Vibrio marinus*. We will refer to the sequence numbering of *V. marinus* TIM (vTIM); according to this numbering, the catalytic residues are Lys-11, His-92, and Glu-169 (see Fig. 2). *V. marinus* is a member of the Vibrionaceae family, able to grow at 4 °C and having an optimal growth temperature of about 15 °C (20). We cloned the gene encoding TIM. Recombinant vTIM was overproduced in *Escherichia coli* and purified. The kinetic properties as well as the stability of the enzyme were determined.

Two structures of this enzyme, one complexed with sulfate and one with the substrate analogue 2-phosphoglycolate (2PG) (Fig. 1), were solved by x-ray crystallography at a resolution of 2.7 Å. Because the sequence of vTIM is most closely related to that of *E. coli* TIM (eTIM) (66% identity) (see Fig. 2), the latter enzyme will be used as a reference for comparison throughout this paper.

Furthermore, sequence comparison of the vTIM sequence with all other known TIM sequences reveals that vTIM has a unique residue in the phosphate binding helix, where the otherwise completely conserved Ser-238 is replaced by an alanine. The implications of this unique sequence feature are discussed by comparing the stability and the kinetic parameters from the native vTIM with its A238S mutant. It turns out that this point mutation decreases the physiological efficiency at 10 °C and it increases the thermal stability, as evidenced by calorimetric studies.

EXPERIMENTAL PROCEDURES

Bacterial Strains and Plasmids—*V. marinus* strain ATCC15382 was obtained from the Laboratorium voor Microbiologie, Universiteit Gent and grown at 15 °C in a medium containing 5 g/liter peptone, 2 g/liter yeast extract, and 25 g/liter marine salt (pH 7.3). *E. coli* BL21 (DE3) cells (*hsd S gal cIts 857 ind1 Sam7 nin5 lacUV-T7*, gene 1) were used for overproduction of the recombinant vTIM. *E. coli* Sure (Stratagene) (*hsd R, mcr A, mcr B, mrr F', pro AB, lacIq, Z M15, Tn10* (*tet*^{r}); Stratagene) and *E. coli* HB101 (*SupE44 hsd S20 rB- mB recA13ara-14 pro A2 lacY1 gal K2rpsL20xyl-5mtl-l*) were used for DNA cloning. The vector used to overexpress the vTIM gene was a derivative of plasmid pT7CTBR (21).

Cloning of the vTIM Gene—A fragment of the vTIM gene was synthesized by polymerase chain reaction using primers corresponding to conserved regions of the molecule (22). This fragment was cloned, ^{32}P-labeled, and used to screen a *V. marinus* genomic library constructed by partially digesting the chromosomal DNA with *Xba*I and ligating the fragments to *Xba*I-cut and dephosphorylated pUC13. A 2,100-bp *Xba*I fragment of *V. marinus* DNA cloned in pUC13 gave a strong hybridization signal with the specific 500-bp polymerase chain reaction fragment used as a probe. DNA sequencing revealed that this 2,100-bp fragment contains the entire TIM gene.

Construction of the Expression Vector—The vTIM gene cloned in pUC13 was digested with *Sau*3AI and *Pst*I. This fragment (about 780 bp) contained the entire TIM gene except for its first 20 codons. These first 20 codons were synthesized chemically with an *Nde*I restriction site adjacent to the initiation ATG codon and a *Sau*3AI protruding end at the opposite site. The resulting oligonucleotide and its complementary strand were annealed, phosphorylated, and ligated to the *Sau*3AI-*Pst*I 780-bp TIM gene fragment as well as to the pT7CTBR plasmid cut with *Nde*I and *Pst*I. The ligation products were used to transform *E. coli* HB101 cells. The correct recombinant plasmid, called pT7-Vib, was used to direct expression of vTIM.

Site-directed Mutagenesis—To construct the gene encoding the A238S mutant of vTIM, site-directed mutagenesis was performed directly on the pT7-Vib vector using the Chameleon kit (Stratagene). The sequence of the mutated oligonucleotide was as follows (5′-3′ noncoding strand; mutated codon underlined): 5′-CTTTTCGCGTCAAGAGATGCGCCGCC-3′ (Eurogentec, Belgium).

Production and Purification of vTIM and Its A238S Mutant—Expression of the TIM gene was performed using the T7 system (23). *E. coli* BL21 (DE3) cells carrying the pT7-Vib recombinant vector were grown for 16 h at 37 °C in L-broth medium containing 100 mg/liter ampicillin. Induction with isopropyl-β-D-thiogalactopyranoside was unnecessary for the production of vTIM and its mutant. The cells were harvested by centrifugation (15 min, 4,500 × *g*) and resuspended in 20 mM Tris-HCl (pH 8.0), 1 mM EDTA. After lysis in a high pressure cell disruption system (Inceltech), the cell debris was removed by centrifugation (45 min, 10,000 × *g*), and the supernatant containing the soluble TIM was recovered. TIM was partially purified by stepwise ammonium sulfate precipitation. Monitoring was performed by SDS-polyacrylamide gel electrophoresis (15% polyacrylamide). TIM precipitated between 60 and 90% saturation. The TIM-containing precipitate was collected by centrifugation (15 min, 20,000 × *g*, 4 °C) and dissolved in 20 mM Tris-HCl (pH 8.0), 1 mM EDTA. The sample was dialyzed against 20 mM triethanolamine-HCl (pH 7.6) overnight at 4 °C. The sample was then concentrated by ultrafiltration with Centricon-10 (Amicon Corp.) and applied onto a Mono Q ion-exchange column (HR 10/10, Pharmacia Biotech Inc.) equilibrated in 20 mM triethanolamine-HCl (pH 7.6). TIM was eluted with a gradient of 0–500 mM NaCl, and the fractions containing TIM were pooled and concentrated with Amicon YM-10 membranes (Amicon). The protein concentration was determined by the method of Bradford (24) using the Bio-Rad protein assay and bovine serum albumin as the standard. An average of 80 mg of TIM was obtained/liter of bacterial culture.

Production and Purification of eTIM—eTIM was produced and purified as described previously (6).

Activity Assays—TIM activity was determined by a coupled enzyme assay based on the decrease of absorbance at 340 nm due to oxidation of NADH, according to Misset and Opperdoes (25). The assay was monitored with a thermostated Uvikon 930 spectrophotometer (Kontron). The reaction mixture (1 ml) contained 0.24 mM NADH (Boehringer Mannheim, Gmbh) and 20 μg/ml glycerol-3-phosphate dehydrogenase (Boehringer Mannheim, Gmbh) in 100 mM triethanolamine-HCl (pH 7.6). To initiate the reaction, 2.5 ng of vTIM or 4 ng of its A238S mutant were added to each sample. The enzymatic assay was performed by adding varied concentrations of the substrate D-glyceralde-

TABLE I
Crystallographic data and refinement statistics of both vTIM structures

	vTIM(sulfate)	vTIM(2PG)
Crystallization buffer	100 mM triethanolamine/HCl	100 mM triethanolamine/HCl
pH	7.0	7.5
Precipitants	1.26 M sodium citrate	2.0 M ammonium sulfate
Additions	1 mM dithiothreitol, EDTA, NaN_3 100 mM ammonium sulfate	1 mM dithiothreitol, EDTA, NaN_3 20 mM 2PG
Space group	$P2_1$	$P2_1$
Cell dimensions (Å)	89.66 137.82 89.54	89.51 138.08 89.52
Cell dimensions (°)	90.00 90.94 90.00	90.00 91.00 90.00
Subunits per asymmetric unit	8	8
V_m (Å^3/Dalton)	2.5	2.5
Data collection statistics		
Observed reflections	166,818	332,463
Unique reflections	60,048	59,692
Overall range (Å)	25–2.65	25–2.70
Overall R-merge (%)	10.1	8.4
Overall completeness (%)	95.7	99.9
Last shell range (Å)	2.70–2.65	2.75–2.70
Last shell R-merge (%)	29.8	19.8
Last shell completeness (%)	95.8	98.2
Refinement		
Protein atoms	3,733	3,733
Ligand atoms	5	18
Solvent atoms	44	77
Resolution range (Å)	8.0–2.65	8.0–2.70
R-factor (%)	20.0	19.2
R-free (%)	21.9	21.5
r.m.s. bond-length deviations (Å)	0.015	0.014
r.m.s. bond angle deviations (°)	1.81	1.70
r.m.s. dihedral angles (°)	24.2	24.5
r.m.s. impropers (°)	1.64	1.50
r.m.s. ΔB for covalently bonded atoms (Å^2)	3.60	3.05
$\chi_1\chi_2$ imperfection (°)[a]	29.1	30.2
Average B-factor, all protein atoms (Å^2)	18.5	12.6
Average B-factor, backbone atoms (Å^2)	17.7	11.7
Average B-factor, side chain atoms (Å^2)	19.5	13.7
Average B-factor, ligand atoms (Å^2)	70.9	27.2
Average B-factor, solvent atoms (Å^2)	28.9	20.2
Ramachandran plot[b]		
Most favored regions (%)	90.3	92.8
Additional allowed regions (%)	8.8	7.0
Generously allowed regions (%)	0.7	0.2
Disallowed regions (%)	0.2	0.0
Noncrystallographic symmetry in dimer		
r.m.s. ΔC_α (Å)	0.45	0.28
r.m.s. $\Delta\varphi$ (°)	22.0	15.9
r.m.s. $\Delta\psi$ (°)	22.2	15.4
r.m.s. ΔB (Å^2)	13.3	8.8

[a] The $\chi_1\chi_2$ imperfection value (6) is the r.m.s. difference between observed $\chi_1\chi_2$ value and the nearest preferred cluster values, as observed in a data base of well refined structures.
[b] As defined by PROCHECK (34).

hyde-3-phosphate (Sigma) (0.13–9.75 mM) to the enzyme system (glycerol-3-phosphate dehydrogenase/NADH) and consecutively measuring the residual activity. Kinetic parameters were determined with the Enzfitter program (26). K_i was measured with 2-phosphoglycolate (2PG) as the inhibitor (27).

Stability Assays—For the stability assays, samples containing 100 mM triethanolamine-HCl (pH 7.6) and TIM were incubated at various temperatures (5–25 °C) in a thermocycler (Programmable TRIO-thermoblock TB-1, Biometra BAU) for 10–60 min. The remaining activity was measured as a function of incubation time. From these measurements an inactivation rate constant, $k_{inact}(sec^{-1})$, was calculated according to Rentier-Delrue *et al.* (22).

Differential Scanning Calorimetry—Thermal unfolding of TIM was studied using a microcal scanning calorimeter differential scanning calorimetric unit (MicroCal, Inc.). Protein samples of 1.3 mg/ml in triethanolamine-HCl buffer (pH 7.6) were used. Samples were heated from 15 to 60 °C, and the scan rate was 1 °C/min.

Crystallization and Data Collection—Crystals were grown at 4 °C using the hanging drop vapor diffusion technique. The protein solutions used in the crystallization setups contained 10 mg/ml protein in 10 mM triethanolamine-HCl, 25 mM NaCl, 1 mM dithiothreitol, 1 mM EDTA, 1 mM NaN_3. For the vTIM(sulfate) crystallization, 100 mM ammonium sulfate was added, and for the vTIM(2PG) crystallization, 20 mM 2PG was added. The crystallization conditions were found using the "Fast Screen" crystallization protocol (28) and are summarized in Table I. Crystals of a size up to $0.3 \times 0.3 \times 0.5$ mm^3 grew within a week, and one of each was used for data collection. Data were collected at 25 °C on a BigMar image plate detector mounted on an Enraf Nonius rotating anode FR571. Data collection was set up to provide a 2.7-Å data set of the vTIM(2PG) crystal and a 2.65-Å data set of the vTIM(sulfate) crystal. The data were processed with DENZO (29). The crystal lattice for both growth conditions is primitive monoclinic. The β-angle for both data sets is about 91° and the a and c cell dimensions are very similar (89.7 and 89.5 Å), agreeing closely with tetragonal symmetry. Indeed at low resolution the data could be merged in space group P4, but for the higher resolution shells this results in an R-merge above 40%. The systematic absences of the 0k0 reflections indicated space group $P2_1$. This symmetry and the cell volume (1.11×10^6 Å^3) suggest that the asymmetric unit contained four TIM dimers, giving a V_m of 2.5 Å^3 Da^{-1}. Data collection statistics for both data sets are shown in Table I.

Molecular Replacement—The molecular replacement calculations were done with the vTIM(sulfate) data set. To find the orientation of the TIM dimers in the unit cell, molecular replacement was performed with the program AMORE (30) using the crystal structure of the eTIM dimer (1TRE; Ref. 6) as the search model. The flexible loop (residues 169–180) known to be variable in conformation was deleted in both monomers. The rotation function showed eight unique solutions, as expected for four dimers per asymmetric unit. A translation function was calculated for each of the eight rotation peaks. The best translation function solution was used to find the position of the second dimer. This proce-

```
                  β1             α1              β2           α2
                <---> *   <--------------->     <--->     <--------->
V.marinus   MRHPVVMGNWKLNGSKEMVVDLLNGLNAELEGVTGVDVAVAPPALFVDLAERTLTEA    57
E.coli      MRHPLVMGNWKLNGSRHMVHELVSNLRKELAGVAGCAVAIAPPEMYIDMAKREAE--    55
Consensus           N K

                β3                     α3      β4                  α4
               <--->               <------->  <--> *         <-------
V.marinus   GSAIILGAQNTDLNNSGAFTGDMSPAMLKEFGATHIIIGHSERREYHAESDEFVAKK    114
E.coli      GSHIMLGAQNVDLNLSGAFTGETSAAMLKDIGAQYIIIGHSERRTYHKESDELIAKK    112
Consensus                   G  TG  S              GH ERR    E       K

                       β5                 α5                   β6
            -------> <---->          <-------------->         <-->*
V.marinus   FAFLKENGLTPVLCIGESDAQNEAGETMAVCARQLDAVINTQGVEALEGAIIAYEPI    171
E.coli      FAVLKEQGLTPVLCIGETEAENEAGKTEEVCARQIDAVLKTQGAAAFEGAVIAYEPV    169
Consensus                C GE                                    YEP

                              α6                  β7          α7
                     <---------------->         <-->       <----->
V.marinus   WAIGTGKAATAEDAQRIHAQIRAHIAEKSEAVAKNVVIQYGGSVKPENAAAYFAQPD    228
E.coli      WAIGTGKSATPAQAQAVHKFIRDHIAKVDANIAEQVIIQYGGSVNASNAAELFAQPD    226
Consensus   W IGTG                                 YGGS

               β8             α8
              <-->     <--------------->
V.marinus   IDGALVGGAALDAKSFAAIAKAAAEAKA                                 256
E.coli      IDGALVGGASLKADAFAVIVKAAEAAKQA                                255
Consensus     G LVG A L
```

FIG. 2. **Sequence alignment of vTIM and eTIM.** The consensus of 45 aligned TIM sequences is also shown. The secondary structure elements of vTIM are indicated. The catalytic residues are indicated by an *asterisk*.

dure was repeated until the positions of all four dimers were found. The R-factor for data between 15 and 3.5 Å for this complete solution was 49.1%, which dropped to 45.7% after rigid body refinement. The correctness of the solution was confirmed by the good packing of the four dimers and the quality of the fit of the omitted loop in the electron density map.

Structure Refinement—First the structure of the vTIM(sulfate) complex was refined. The sequence of the molecular replacement model was mutated from that of eTIM to that of vTIM in both monomers. The model was optimized to improve its fit in a 2Fo-Fc SIGMA A weighted map (CCP4; Ref. 31) using O (32) running on an Evans and Sutherland workstation. For refinement, a subset of 5% of the data (the test set) was used for R-free calculations. Refinement was pursued with a mixture of simulated annealing x-ray refinement and conventional positional and thermal factor refinement using the X-PLOR package (33) for all refinement calculations. The positions and the thermal B-factors of the atoms of both monomers in the dimer were refined independently. The atom positions of the three other dimers were generated by strict noncrystallographic symmetry operators, recalculated at several stages of the refinement by rigid body refinement.

Electron density maps indicated an open conformation for loop 6, which was manually rebuilt into the density. In addition, a sulfate ion was found in the active site of the first subunit. Its coordinates were included in the model. In the final stages of the refinement, water molecules were added at sites, displaying a peak larger than 3 S.D. above the mean in an Fo-Fc map and having a potential hydrogen bonding partner. In total, 44 water molecules were added per dimer. The final R-factor was 20.3% and R-free was 22.0% to a resolution of 2.65 Å (Table I).

Subsequently this structure was used for the rigid body refinement against the vTIM(2PG) data set. Electron density maps showed clear density for the closed loop 6 and the 2PG bound in the active site of both subunits. A similar protocol as for the native structure refinement was used, loop 6 was rebuilt, the inhibitor 2PG was built into the active site of both subunits, and 77 waters per dimer were added. It resulted in a final R-factor of 19.2% (R-free is 21.5%) for this vTIM(2PG) structure. The refinement statistics are given in Table I.

Structure and Sequence Analysis—The quality of the structures was analyzed using the programs PROCHECK (34) and WHAT IF (35). For the purpose of analysis, TIM structures were superimposed on the basis of the 129 C_α positions forming the eight α-helices and eight β-strands using the lsq option in O. Cavities were calculated with the program MSP (36), intermolecular contacts were calculated with WHAT IF, and molecular graphs were drawn with the programs MOLSCRIPT (37) (Fig. 6) and ICM[4] (38) (Figs. 7 and 8). The consensus sequence shown in Fig. 2 was obtained from a sequence alignment of 45 sequences currently available in the data bases using PILEUP (39) as well as a superposition analysis of known structures.

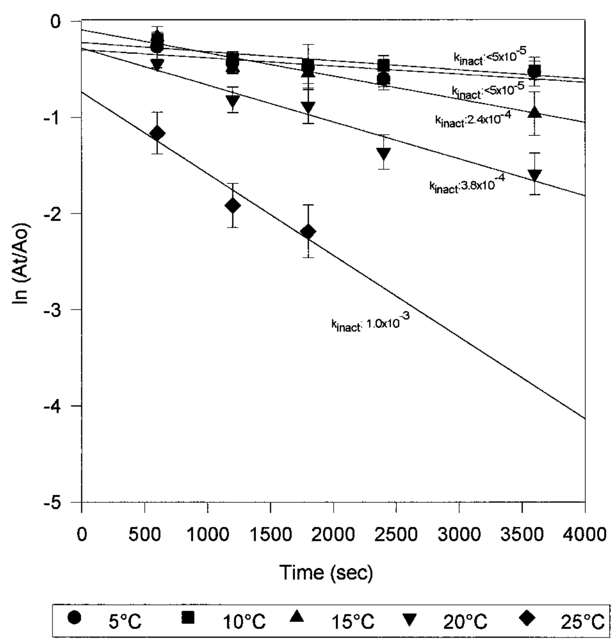

FIG. 3. **Inactivation rate constants of vTIM measured at different temperatures.** The k_{inact} value (sec^{-1}) is defined as the slope of the ln(*At/Ao*) *versus* the incubation time (22).

RESULTS AND DISCUSSION

Kinetic and Stability Properties of vTIM

In the present work we have cloned the gene encoding TIM of *V. marinus*. The corresponding protein was expressed in *E. coli*. The thermostability of this recombinant TIM was assessed by measuring the inactivation rate constant (k_{inact}) at various temperatures (Fig. 3). At 25 °C the value recorded was 1 × 10^{-3} sec^{-1}. The calculated half-life ($t_{1/2}$) was 10 min at this temperature, showing the intrinsic psychrophilic character of this TIM. Because of its psychrophilic properties, we choose to measure its kinetic parameters at 10 °C; at this temperature $t_{1/2}$ is 58 min. The kinetic properties are summarized in Table II.

It is interesting to point out that the k_{cat} (vTIM, 10 °C) is very similar to the k_{cat} (eTIM, 25 °C), as shown in Table II. An important difference between vTIM and eTIM is the K_i (2PG), which for vTIM is approximately 10 times higher, showing that

[4] http://molsoft.com.

TABLE II
Kinetic parameters (for the conversion of D-glyceraldehyde-3-phosphate into dihydroxyacetone phosphate) and stability data of vTIM, its A238S variant, and eTIM

The kinetic parameters of vTIM and its A238S variant were determined at 10 °C, whereas those of eTIM were measured at 25 °C. $t_{1/2}$ values were calculated with data as shown in Fig. 3; T_d, the temperature of half-denaturation, was determined from Fig. 4.

	Unit	vTIM	A238S	eTIM
Kinetic data				
K_m	mM	1.9 ± 0.2	4.8 ± 0.6	1.03 ± 0.1
k_{cat}	min^{-1}	4.2 ± 0.1 × 10^5	2.8 ± 0.1 × 10^5	5.4 ± 0.1 × 10^5
k_{cat}/K_m	min^{-1} mol^{-1}	2.2 ± 0.2 × 10^5	0.6 ± 0.06 × 10^5	5.2 ± 0.6 × 10^5
K_I (2PG)	mM	89	101	6
Stability data				
$t_{1/2}$ (T = 25 °C)	min	10	27	NA[a]
T_d	°C	41	46	54

[a] NA, not applicable. These data were not measured because thermal inactivation of eTIM is undetectable at these temperatures (22).

the affinity of the vTIM active site for 2PG is much weaker. It is not clear from the structure how to explain this difference. For example an analysis of the presence of the charged side chains within a sphere of radius 8 Å from the phosphate position showed no difference between vTIM and eTIM, except for the presence of an asparagine at position 216 in eTIM, where in vTIM a lysine is found (the NZ atom is at a distance of 7.1 Å from the phosphate). The Asn-216 in eTIM is responsible for the N-capping of helix 7, whereas in vTIM Pro-217 has the same role.

Characterization of the A238S Mutant

To assess the role of the unique Ala-238 in loop 8 of vTIM, we decided to study the point mutant A238S. The mutant was produced and purified in the same manner as the native TIM. Its catalytic efficiency and its stability were analyzed (Table II). Activity measurements at different temperatures revealed that the mutant has a higher thermal stability than the corresponding wild type; for example the half-lifes of wild type and A238S at 25 °C are 10 and 27 min, respectively (Table II). This was confirmed by microcalorimetric studies (Fig. 4), showing that thermal unfolding of the mutant occurs at higher temperatures. In both cases, denaturation was found to be irreversible under the conditions tested. The values of the temperature of half-denaturation T_d, calculated for a protein concentration of 1.3 mg/ml, were 40.8 °C for the wild type enzyme and 45.8 °C for the mutant.

The kinetic parameters of the A238S mutant were determined at 10 °C and are compared with those of the wild type vTIM and eTIM (Table II). The mutant has a k_{cat} value that is somewhat lower than that observed for the wild type, whereas its K_m is somewhat higher, implying that the mutant is 3.8 times less efficient at 10 °C. The K_i (2PG) for wild type and mutant is rather similar. These data demonstrate that an alanine at position 238 contributes to a lower thermal stability (more psychrophilic) but allows for a higher catalytic efficiency at low temperatures.

X-ray Structure

The vTIM(sulfate) Structure—The model of vTIM consists of residues 2–250 for subunit A and subunit B. The N-terminal methionine was not included in the model because the electron density map was not clear in this region in both subunits. Nevertheless, the highest peak in the final (Fo-Fc) α_c map is at the N termini of both subunits, in agreement with the notion that the methionine is present but disordered.

The stereochemical quality of the refined structure was analyzed with the program PROCHECK (34). All stereochemical parameters for the main chain and side chain atoms are better than those for proteins refined to a similar resolution. The Ramachandran plot shows all the residues in the allowed regions of conformational space with one exception. The catalytic

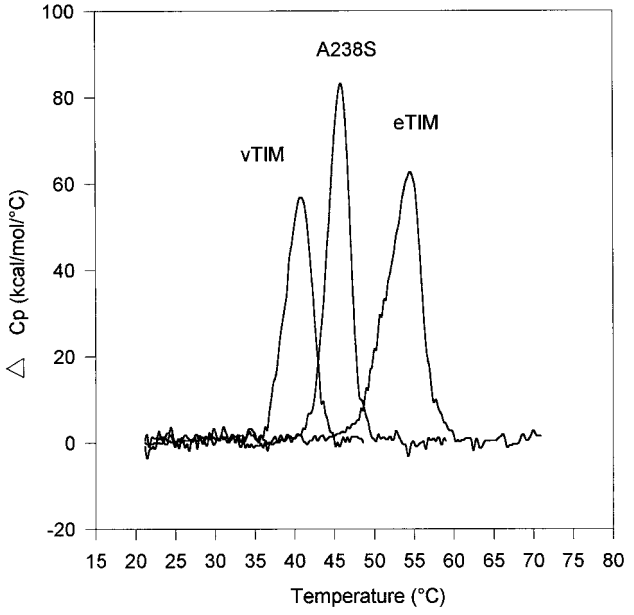

FIG. 4. **Thermogram of vTIM, A238S, and eTIM.** The change in heat capacity (ΔCp) is represented as a function of the temperature.

residue Lys-11 has an unusual conformation in both subunits ($\varphi \approx 58°$; $\psi \approx 140°$), although it has low B values and is well determined in the electron density. The lysine residue has to adopt this unusual conformation to position its side chain at a very precise location in the active-site pocket, a general feature seen in all TIM structures.

In Fig. 5 the real space density correlation coefficient for the main chain atoms is displayed as a function of residue number for both monomers. The lowest values are found in loop 6, which is poorly defined in the electron density map. Loop 6 has the highest B-factors as also shown in Fig. 5. The B-factors of the second subunit are consistently higher than the B-factors of the first subunit. This is due to the different packing interactions; for each of the dimers in the asymmetric unit it is observed that the first subunit has more crystallographic contacts when compared with the second subunit. For the first subunit approximately 45 intermolecular contacts are observed, and for the second subunit only 23 (when using a cutoff of 3.5 Å) are observed.

Both subunits are very similar with a C_α r.m.s. deviation of 0.29 Å for the framework C_α atoms and of 0.45 Å for all main chain C_α atoms. Loop 6 is in the open conformation, and Glu-169 adopts the swung-out conformation (19), contacting Ser-98 of loop 4. A sulfate ion occupies the active-site pocket of subunit A but not of subunit B. The average thermal B-factor of the atoms of this ion is high (70 $Å^2$), suggesting a low occupancy of this site.

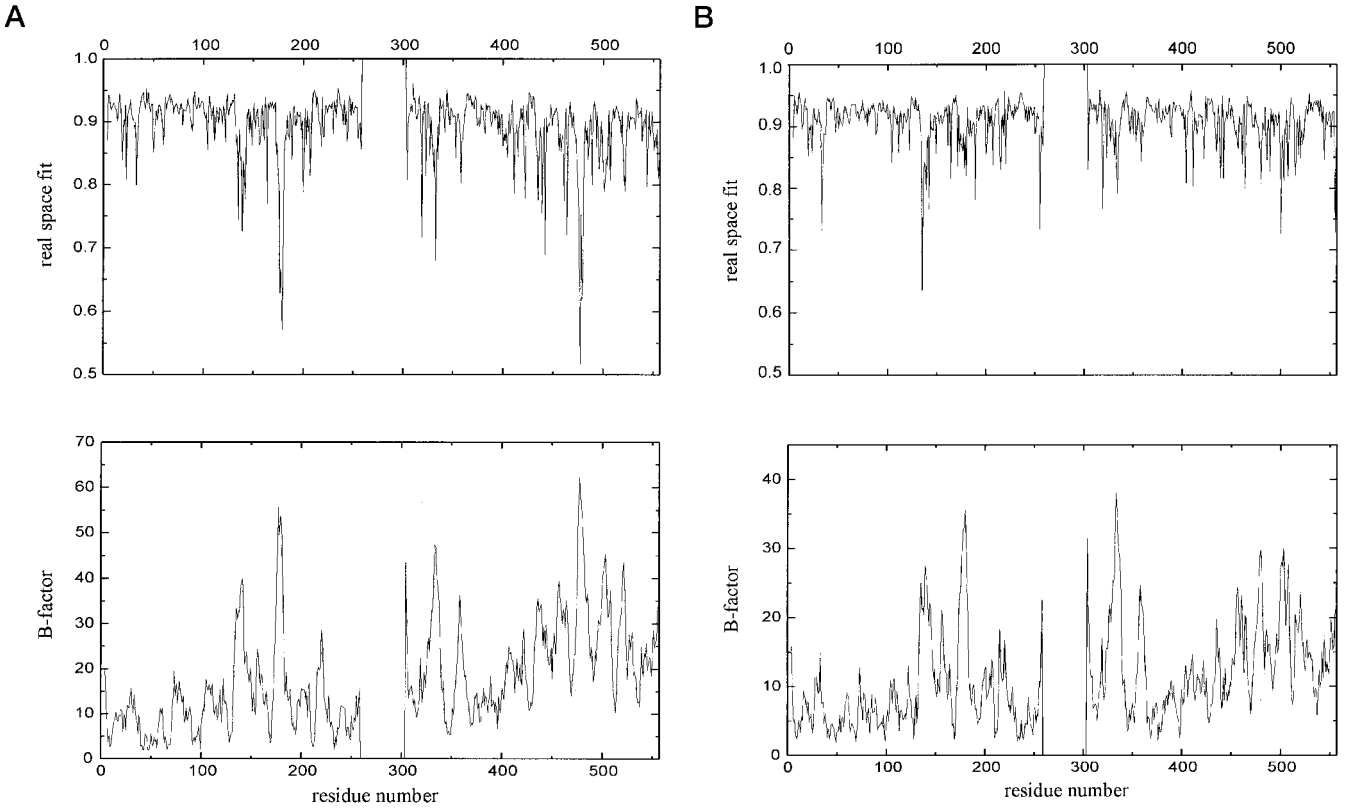

FIG. 5. **Real space fit (*top*) and average B-factor (Å^2) for the main chain atoms (*bottom*) for the vTIM(sulfate) (*A*) and vTIM(2PG) (*B*) structure.** The residue numbering of the first and second subunit starts at 2 and 302, respectively.

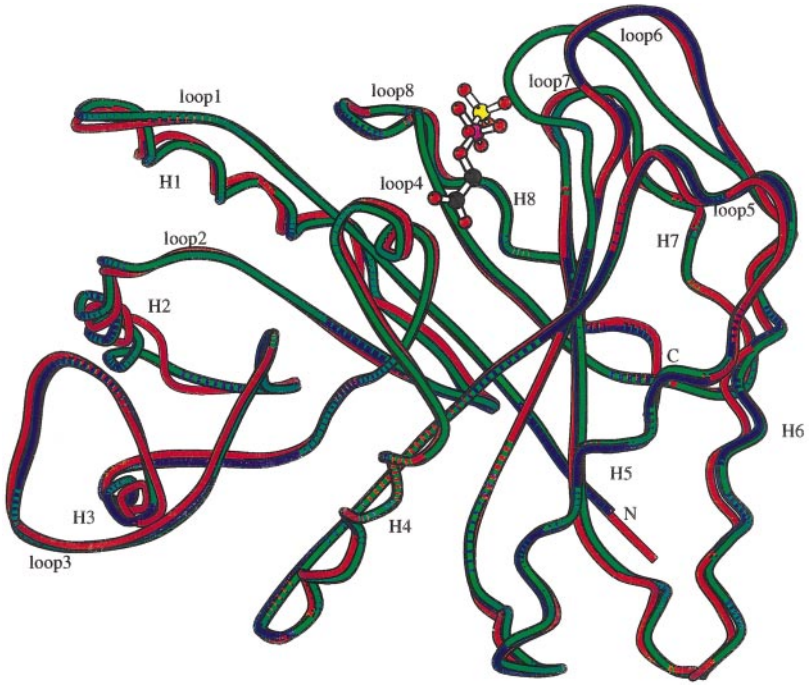

FIG. 6. **Superposition of the backbone of the vTIM(2PG) (*green*), vTIM-(sulfate) (*blue*), and eTIM (*red*) structures.** The sulfate ion and the 2PG molecule are also shown, indicating the difference in position of the P atom (*pink*), and the S atom (*yellow*). Loop 6 of the vTIM(2PG) structure is in the closed conformation. *N* and *C* identify the N terminus and C terminus, respectively.

The vTIM(2PG) Structure—The structure of vTIM(2PG) is very similar to the structure of vTIM(sulfate), with a C_α r.m.s. deviation of 0.18 Å for the framework C_α atoms and of 0.95 Å for all main chain C_α atoms of the first monomer. The most important differences are the presence of 2PG in both active sites of the dimer and, consequently, the closed conformation of loop 6 in both subunits (Fig. 6). In the vTIM(2PG) structure, loop 6 is well defined by the electron density map, and the loop 6 atoms do have lower B-factors when compared with the vTIM(sulfate) structure (Fig. 5). The catalytic glutamate, Glu-169, at the beginning of loop 6 is now seen in the swung-in conformation, contacting the 2PG molecule, as already seen in other TIM complexes. The 2PG phosphate position does not exactly superimpose on the sulfate of the vTIM(sulfate) structure. The distance between the equivalent S and P atoms is 1.25 Å. As shown in Fig. 6, the phosphate moiety is bound

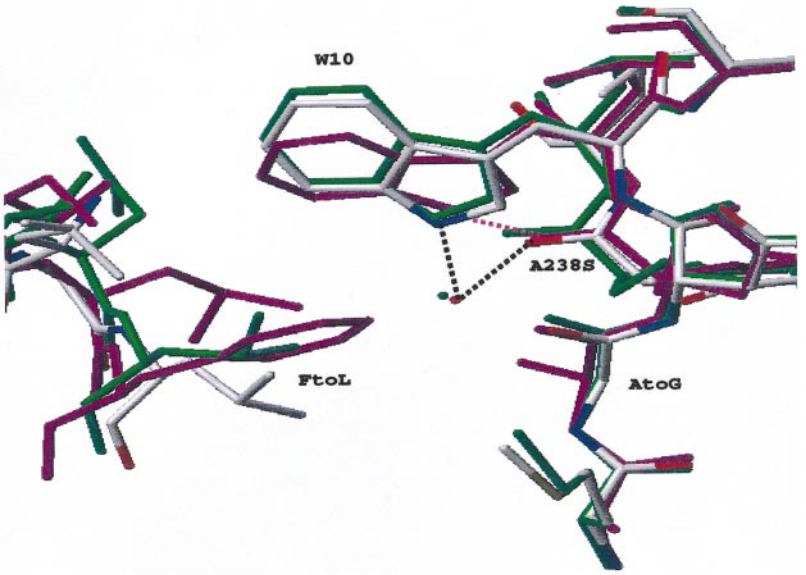

FIG. 7. **Superposition of the vTIM-(sulfate) (color coded according to atom type), eTIM (*green*) and tTIM (*purple*) structure, comparing the water-mediated bond (*black*) between NE1 of Trp 10 and O of residue 238 in vTIM and eTIM with the direct hydrogen bond (*purple*) in tTIM.** The water positions are indicated by a *red dot* (vTIM) and a *green dot* (eTIM). Note the AtoG and FtoL sequence difference between tTIM and the two other TIMs at positions 8 and 26, respectively.

deeper into the active-site pocket. This fact has also been seen in similar complexes of trypanosomal TIM (tTIM) (19).

Comparison of the vTIM with the eTIM Structure—The sequences of vTIM and eTIM have almost the same length (256 for vTIM and 255 for eTIM) with a quite high sequence homology (66% sequence identity), suggesting a close evolutionary relationship. There is only one insertion of two residues at the C-terminal end of helix α2 (Fig. 1), resulting in a longer helix α2 in vTIM (Fig. 6). This difference is located at the N-terminal end of the β-barrel, and concerns residues not involved in catalysis and dimer formation. The overall fold of both vTIM structures and the unliganded eTIM structure has been compared in Fig. 6. The rms difference after superposition of the 129 framework C_α atoms of the vTIM(sulfate) and the eTIM structures is 0.59 Å for these framework atoms. A detailed structural analysis of the eTIM structure has shown some unique structural features (6), the majority of which are also present in vTIM. For example in vTIM and eTIM a methionine is located at position 7 in strand β1, where in other known TIM structures a glycine or an alanine is located. This methionine points into the interior of the barrel. The larger space required is compensated for by smaller residues in the environment. Another unique common feature of vTIM and eTIM is found in the region between loop 1 and loop 8, as shown in Fig. 7, in which the structures of vTIM, eTIM, and tTIM are superimposed. A buried water molecule is observed in this region in vTIM and eTIM, hydrogen-bonded to NE1(Trp-10) and O(Ala-238). The presence of this water molecule does correlate with two sequence changes in this region; in particular it concerns the mutation of an alanine (in tTIM) to a glycine (in vTIM and eTIM) at position 8 and of a phenylalanine (in tTIM) to a leucine (in vTIM and eTIM) at position 26. As a result of these two changes to a smaller side chain, a cavity is formed that is filled up by a water molecule. A small rotation of the Trp side chain is also observed. Consequently, the direct hydrogen bond of NE1(Trp10) and O(238) between loop 1 and loop 8 as seen in tTIM is replaced by the above-mentioned water-mediated hydrogen bond (Fig. 7). Another common feature of vTIM and eTIM is an intersubunit salt bridge between residue 79 and His-104 that is not observed in the other structures, where an intersubunit salt bridge exists between Glu-79 and Arg-100. The latter contact is absent in eTIM due to a reorientation of the side chains from the residues involved. In vTIM an aspartate is found at the position of Glu-79 in eTIM, and the previously mentioned salt bridge between residue 79 of one subunit

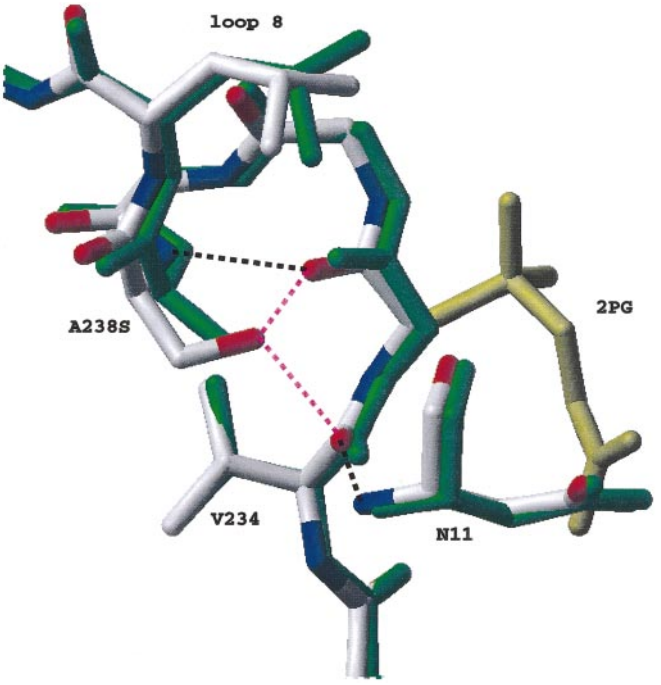

FIG. 8. **Superposition of loop 8 of eTIM (color coded according to atom type) and vTIM(2PG) (all atoms colored *green*).** The *dotted lines* show the hydrogen bonding interactions of OG(Ser), O(234), and O(235) as seen in eTIM. The *purple* hydrogen bonds are absent in vTIM. The 2PG molecule (all atoms colored *yellow*) is also shown for reason of reference. Similar view as Fig. 6.

and residue 100 of the other subunit is also present, as well as the Asp-79–His-104 salt bridge.

There are three unique residues in vTIM when compared with the other nine known structures: Asp-79, Ala-182, and Ala-238. Only the latter is a unique residue when comparing the 45 known sequences of TIM. Position 79 is at the tip of loop 3; in most sequences (41 times) this is a glutamate involved in an intersubunit contact as discussed above; sometimes an aspartate (three times) or a threonine (one time) is observed. Position 182 is at the N terminus of helix 6; in most other sequences a proline (34 times) is seen at this N-cap position, but in some sequences a glycine (1 time), an alanine (6 times), a threonine (2 times), a valine (1 time), or an asparagine (1 time) is observed. As previously mentioned, at position 238 an

alanine is found in vTIM, where in all the other sequences a serine is observed. The importance of Ala-238 is discussed in the next section.

The A238S Mutation in the Phosphate Binding Helix—Position 238 is at the beginning of the conserved phosphate binding 3/10 helix in loop 8. The structural and stability effects of an alanine to serine mutation has been studied in at least two other well characterized proteins: lysozyme and barnase (40, 41). In all studied examples, the structural changes of this mutation are minimal. In none of the cases does the mutation significantly enhance the stability; moreover in almost all cases this mutation is destabilizing. The effects depend on the structural context of the mutated alanine; for fully exposed alanines, the mutation into a serine does only have minimal effects on the stability, but for fully buried alanines, the new variants are much less stable (41). The alanine to serine mutation in vTIM causes a significant increase in stability. This can be understood from the structural context of Ala 238 in vTIM. The C_β atom of Ala-238 is completely buried inside the protein interior, as is the serine side chain in the other TIM structures. Loop 8 of vTIM does superimpose very well on loop 8 of the other TIMs. Only small rearrangements are seen (Fig. 8). As a result no cavity can be detected in this region of the vTIM structure. Apparently the loop 8 helix is very rigid, as seen from the B-factor plot in Fig. 5. Important for the structure comparison is the observation that in the other TIMs, for example eTIM (Fig. 8), the buried O_γ atom of the conserved serine makes two hydrogen bonds to main chain oxygen atoms. As can be seen in Fig. 8, each of these two buried main chain oxygens is making another hydrogen bond with a neighboring main chain peptide NH. These hydrogen bonds are also present in wild type vTIM. Assuming no major structural rearrangements, the alanine to serine mutation in vTIM will generate two additional buried hydrogen bonds, which rationalizes the extra stability of this variant (Table II). The assumption of only minor structural rearrangements is entirely consistent with the observation that the kinetic properties of vTIM and A238S are rather similar. The increase in stability, as expressed in a T_d increase of approximately 5 °C is quite significant. For example it is larger than the most stabilizing point mutation observed in more than 190 lysozyme variants (only 48 stabilizing, from which only 4 with an increase of T_d higher than 1.5 °C and with a maximum of 2.8 °C) (42). This is partly due to the fact that TIM is a dimer; therefore the more favorable hydrogen bond interactions occur twice. Furthermore it is also due to the very good hydrogen bonding complementarity of the environment for a serine at this site (Fig. 8).

Concluding Remarks—In this paper we reported the purification and the kinetic and stability properties of triose-phosphate isomerase from the psychrophilic bacterium *V. marinus* and its A238S mutant as well as two x-ray structures of the native enzyme, one complexed with sulfate and one complexed with the substrate analogue 2PG. The vTIM structure is very similar to the structure of eTIM, in agreement with the high sequence identity. The comparison of the structures of vTIM and eTIM does not provide an explanation for the 10-fold lower affinity of 2PG for vTIM, when compared with eTIM. One unique sequence feature of vTIM has been found, which is Ala-238, whereas in all other TIM sequences a serine is observed. The importance of the alanine at position 238 has been investigated further by studying the properties of the A238S mutant. A238S is considerable more stable than wild type, and it catalyzes the reaction less efficiently; therefore, there is good evidence that the alanine at position 238 is a successful adaptation to the psychrophilic character of *V. marinus*.

Acknowledgments—We acknowledge the important technical assistance of M. Lion and J. M. Rotsaert. We thank Dr. S. C. Mande for his help in analyzing the effect of the A238S replacement. D. M. thanks the EMBL in Heidelberg, where part of this work was carried out.

REFERENCES

1. Knowles, J. R. (1991) *Nature* **350,** 121–124
2. Neria, E., and Karplus, M. (1997) *Chem. Phys. Lett.* **267,** 23–30
3. Banner, D. W., Bloomer, A. C., Petsko, G. A., Philips, D. C., Pogson, C. I., Wilson, I. A., Corran, P. H., Furth, A. J., Milman, J. D., Offord, R. E., Priddle, J. D., and Waley, S. G. (1975) *Nature* **255,** 609–614
4. Lolis, E., Alber, T., Davenport, R. C., Rose, D., Hartman, F. C., and Petsko, G. A. (1990) *Biochemistry* **29,** 6609–6618
5. Wierenga, R. K., Noble, M. E. M., Vriend, G., Nauche, S., and Hol, W. G. J. (1991) *J. Mol. Biol.* **220,** 995–1015
6. Noble, M. E. M., Zeelen, J. Ph., and Wierenga, R. K (1993) *Acta Crystallogr. Sec. D* **49,** 403–417
7. Mande, S. C., Mainfroid, V., Kalk, K. H., Goraj, K., Martial, J. A., and Hol, W. G. J. (1994) *Protein Sci.* **3,** 810–821
8. Delboni, L. F., Mande, S. C., Rentier-Delrue, F., Mainfroid, V., Turley, S., Vellieux, M. D., Martial, J. A., and Hol, W. G. J. (1995) *Protein Sci.* **4,** 2594–2604
9. Velanker, S. S, Ray, S. S., Gokhale, R. S., Hemalatha Balaram, S. S., and Murthy, M. R. N. (1997) *Structure* (*Lond.*) **5,** 751–761
10. Reardon, D., and Farber, G. K. (1995) *FASEB J.* **9,** 497–503
11. Borchert, T. V., Abagyan, R. A., Radha Kishan, K. V., Zeelen, J. Ph., and Wierenga, R. (1993) *Structure* **1,** 205–213
12. Thanki, N., Zeelen, J. Ph., Mathieu, M., Jaenicke, R., Abagyan, R. A., Wierenga, R. K., and Schliebs, W. (1997) *Protein Eng.* **10,** 159–167
13. Goraj, K., Renard, A., and Martial, J. A. (1990) *Protein Eng.* **3,** 259–266
14. Tanaka, T., Kimura, H., Hayashi, M., Fujiyoshi, Y., Fukuhara, K., and Nakamura, H. (1994) *Protein Sci.* **3,** 419–427
15. Urfer. R., and Kirschner, K. (1992) *Protein Sci.* **1,** 31–45
16. Schliebs, W., Thanki, N., Eritja, R., and Wierenga, R. (1996) *Protein Sci.* **5,** 229–239
17. Wierenga, R. K., Noble, M. E. M., Postma, J. P. M., Groendijk, H., Kalk, K. H., Hol, W. G. J., and Opperdoes, F. R. (1991) *Proteins* **10,** 33–49
18. Joseph, D., Petsko, G. A., and Karplus, M. (1990) *Science* **249,** 1425–1428
19. Noble, M. E. M., Zeelen, J. Ph., and Wierenga, R. K. (1993) *Proteins* **16,** 311–326
20. Morita, R. Y. (1975) *Bacteriol. Rev.* **39,** 144–167
21. L'Hoir, C., Renard, A., and Martial, J. A. (1990) *Gene* **89,** 47–52
22. Rentier-Delrue, F., Mande, S. C., Moyens, S., Terpstra, P., Mainfroid, V., Goraj, K., Hol, W. G. J., and Martial, J. A. (1993) *J. Mol. Biol.* **229,** 85–93
23. Studier, F. W., and Moffat, B. A. (1986) *J. Mol. Biol.* **189,** 113–130
24. Bradford, M. M. (1976) *Anal. Biochem.* **72,** 248–254
25. Misset, O., and Opperdoes, F. (1984) *Eur. J. Biochem.* **144,** 475–483
26. Leatherbarrow, R. J. (1987) *ENZFITTER: A nonlinear Regression Data Analysis Program for the IBM PC/P52*, Elsevier Biosoft, Cambridge, UK
27. Wolfenden, R. (1969) *Nature* **233,** 704–705
28. Zeelen, J. Ph., Hiltunen, J. K., Ceska, T. A., and Wierenga, R. K. (1994) *Acta Crystallogr. Sec. D* **50,** 443–447
29. Otwinowski, Z. (1993) *DENZO: An Oscillation Data Processing Program for Macromolecular Crystallography,* Yale University Press, New Haven, CT
30. Navazza, J. (1994) *Acta Crystallogr. Sec. A* **50,** 157–163
31. Collaborative Computational Project No. 4 (CCP4) (1994) *Acta Crystallogr. Sec. D* **50,** 760–763
32. Jones, T. A., Zou, J. Y., Cowan, S. W., and Kjeldgaard, M. (1991) *Acta Crystallogr. Sec. A* **47,** 110–119
33. Brünger, A. T. (1992) *X-PLOR: A System For X-ray Crystallography and NMR,* Version 3.1, Yale University Press, New Haven, CT
34. Laskowski, R. A., MacArthur, M. W., Moss, D. S., and Thornton, J. M. (1993) *J. Appl. Crystallogr.* **26,** 283–291
35. Vriend, G. (1990) *J. Mol. Graphics* **8,** 52–56
36. Conolly, M. L. (1985) *J. Am. Chem. Soc.* **107,** 1118–1124
37. Kraulis, P. J. (1991) *J. Appl. Crystallogr.* **24,** 946–950
38. Abagyan, R. A. (1977) *The ICM*, Version 2.6, Molsoft LLC, New York
39. Devereux, J., Haeberli, P., and Smithies, O. (1984) *Nucleic Acids Res.* **12,** 387–395
40. Serrano, L., Sancho, J., Hirshberg, M., and Fersht, A. R. (1992) *J. Mol. Biol.* **227,** 544–559
41. Blaber, M., Lindstrom, J. D., Gassner, N., Xu, J., Heinz, D. W., and Matthews, W. (1993) *Biochemistry* **32,** 11363–11373
42. Matthews, B. W. (1995) *Adv. Protein Chem.* **46,** 249–277